



Temporal changes in surface partial pressure of carbon dioxide and carbonate saturation state in the eastern equatorial Indian Ocean during the 1962–2012 period

L. Xue¹, W. Yu¹, H. Wang¹, L.-Q. Jiang², L. Feng¹, L. Gao¹, K. Li¹, Z. Li¹, Q. Wei³, and C. Ning¹

¹Center for Ocean and Climate Research, First Institute of Oceanography, State Oceanic Administration, Qingdao 266061, China

²Cooperative Institute for Climate and Satellites–Maryland, Earth System Science Interdisciplinary Center, University of Maryland, College Park, Maryland 20740, USA

³Marine Ecology Research Center, First Institute of Oceanography, State Oceanic Administration, Qingdao 266061, China

Correspondence to: L. Xue (xueliang@fio.org.cn)

Received: 13 December 2013 – Published in Biogeosciences Discuss.: 8 January 2014

Revised: 22 September 2014 – Accepted: 20 October 2014 – Published: 21 November 2014

Abstract. Information on changes in the oceanic carbon dioxide (CO₂) concentration and air–sea CO₂ flux as well as on ocean acidification in the Indian Ocean is very limited. In this study, temporal changes of the inorganic carbon system in the eastern equatorial Indian Ocean (EIO, 5° N–5° S, 90–95° E) are examined using partial pressure of carbon dioxide ($p\text{CO}_2$) data collected in May 2012, historical $p\text{CO}_2$ data since 1962, and total alkalinity (TA) data calculated from salinity. Results show that sea surface $p\text{CO}_2$ in the equatorial belt (2° N–2° S, 90–95° E) increased from $\sim 307 \mu\text{atm}$ in April 1963 to $\sim 373 \mu\text{atm}$ in May 1999, $\sim 381 \mu\text{atm}$ in April 2007, and $\sim 385 \mu\text{atm}$ in May 2012. The mean rate of $p\text{CO}_2$ increase in this area ($\sim 1.56 \mu\text{atm yr}^{-1}$) was close to that in the atmosphere ($\sim 1.46 \mu\text{atm yr}^{-1}$). Despite the steady $p\text{CO}_2$ increase in this region, no significant change in air–sea CO₂ fluxes was detected during this period. Ocean acidification as indicated by pH and saturation states for carbonate minerals has indeed taken place in this region. Surface water pH (total hydrogen scale) and saturation state for aragonite (Ω_{arag}), calculated from $p\text{CO}_2$ and TA, decreased significantly at rates of -0.0016 ± 0.0001 and $-0.0095 \pm 0.0005 \text{ yr}^{-1}$, respectively. The respective contributions of temperature, salinity, TA, and dissolved inorganic carbon (DIC) to the increase in surface $p\text{CO}_2$ and the decreases in pH and Ω_{arag} are quantified. We find that the increase in DIC dominated these changes, while contribu-

tions from temperature, salinity, and TA were insignificant. The increase in DIC was most likely associated with the increasing atmospheric CO₂ concentration, and the transport of accumulated anthropogenic CO₂ from a CO₂ sink region via basin-scale ocean circulations. These two processes may combine to drive oceanic DIC to follow atmospheric CO₂ increase.

1 Introduction

Over the past decade, the global ocean took up atmospheric carbon dioxide (CO₂) at a rate of about 2.5 Pg C yr^{-1} ($1 \text{ Pg} = 10^{15} \text{ g}$), roughly a quarter of all the anthropogenic CO₂ released from fossil fuel burning, cement production, and land-use change (Le Quéré et al., 2014). The oceans' uptake of atmospheric CO₂ plays an important role in slowing down the increase of atmospheric CO₂ (Sabine et al., 2004; Takahashi et al., 2009) and hence the global climate change. Therefore, it is important to accurately document changes of the oceanic CO₂ sink in order to accurately project future atmospheric CO₂ levels and global climate change (Takahashi and Sutherland, 2013).

The oceanic CO₂ sink is mainly controlled by the gradient of the partial pressure of CO₂ ($p\text{CO}_2$) between the atmosphere and the ocean ($\Delta p\text{CO}_2 = p\text{CO}_2 \text{ water} - p\text{CO}_2 \text{ air}$).

Considering that the spatiotemporal variability of atmospheric $p\text{CO}_2$ is much smaller than that of the surface water $p\text{CO}_2$, one could assume that the magnitude of $\Delta p\text{CO}_2$ and hence the net air–sea CO_2 flux are governed primarily by oceanic $p\text{CO}_2$ (Takahashi and Sutherland, 2013). While atmospheric CO_2 levels increased from ~ 280 ppm (parts per million by volume) in the preindustrial era to ~ 393 ppm in 2012 almost homogeneously across the globe (Tans and Keeling, 2013), oceanic $p\text{CO}_2$ showed different rates of change depending on local oceanographic processes (e.g., lateral mixing, upwelling, and biological activity) (Takahashi et al., 2006). For instance, Le Quéré et al. (2009) found that the $p\text{CO}_2$ increase rate in the North Atlantic was larger than that in the atmosphere during the 1981–2007 period, while the $p\text{CO}_2$ increase rate in the North Pacific was smaller than that in the atmosphere. Even a decrease in sea surface $p\text{CO}_2$ was observed in the vicinity of the Bering and Okhotsk seas between 1970 and 2004 (Takahashi et al., 2006). Consequently, the oceanic CO_2 sink also exhibited different trends. For example, a decrease in the sink for atmospheric CO_2 was observed in the North Atlantic subpolar gyre (50 – 70° N, 80 – 10° W) from 1982 to 1998 (Lefèvre et al., 2004), whereas a large increase of the CO_2 sink was found in the western tropical North Atlantic (19 – 20° N, 65 – 68° W) from 2002 to 2009 (Park and Wanninkhof, 2012). It is therefore crucial to determine changes in sea surface $p\text{CO}_2$ in local regions to better understand changes and variability in the global oceanic carbon sink.

While effectively alleviating the global climate change, the oceans' uptake of atmospheric CO_2 is taking a toll on the world's oceans (Doney et al., 2009). It causes decreasing pH, carbonate ion concentrations, and carbonate mineral saturation states, a process commonly termed “ocean acidification” (OA) (Caldeira and Wickett 2003; Feely et al. 2004; Orr et al. 2005). The pH decline can induce speciation shifts of major and minor elements in seawater, affecting their bioavailability to phytoplankton (Doney et al., 2009). The decrease of calcium carbonate (CaCO_3) saturation state could affect the ability of marine calcifying organisms to form their CaCO_3 shells and skeletons.

The Indian Ocean, strongly influenced by seasonal monsoonal forcing (Schott and McCreary, 2001), is a unique basin with highly variable oceanic circulation and multi-scale air–sea interaction processes (Schott et al., 2009). It plays an important role in the global biogeochemical cycling of carbon and nutrients (e.g., Wiggert et al., 2009). Much effort has been devoted to this region to understand distributions of inorganic carbon parameters and their controlling processes as well as the region's role in the global carbon cycle. Activities have been primarily propelled by several national or international programs, such as the Joint Global Ocean Flux Study (JGOFS) and the World Ocean Circulation Experiment (WOCE) (e.g., Naqvi, 2002; Sabine et al., 2002; Bates et al. 2006).

Nevertheless, the oceanic $p\text{CO}_2$ change and its influence on the oceanic CO_2 sink in the Indian Ocean are far from well documented when compared to those in the Pacific and Atlantic oceans (Takahashi et al., 2009; Lenton et al., 2012; Fay and McKinley, 2013; Sarma et al., 2013). Furthermore, many of the existing studies in the region are based on model results (e.g., Sarma et al., 2013; Valsala and Maksyutov, 2013), which may not well reflect the real situation. For instance, a recent study, based on ocean biogeochemical models, suggested a small enhancement in the CO_2 sink during the 1990–2009 period in the southern Indian Ocean (Sarma et al., 2013), even though Metzl (2009) observed that oceanic $p\text{CO}_2$ increased at a rate of $2.11 \pm 0.07 \mu\text{atm yr}^{-1}$ during the 1991–2007 period in the southwestern Indian Ocean and the corresponding Antarctic sector (implying a reduction in the oceanic CO_2 sink). It is worthwhile to conduct more studies using in situ observations in the Indian Ocean to better understand the change of surface $p\text{CO}_2$ and the oceanic CO_2 sink in the Indian Ocean.

Furthermore, surface water pH in the Indian Ocean is relatively low, when compared to other oceans (Takahashi and Sutherland, 2013). This, combined with the fact that corals are widely distributed in the region (Allen and Adrim, 2003), makes the Indian Ocean one of the most vulnerable regions in terms of OA. However, relatively little information on OA is available in the Indian Ocean. It is urgent to examine the changes of pH and CaCO_3 saturation state in the Indian Ocean and their potential influence on marine organisms.

In this paper, we report an oceanic $p\text{CO}_2$ increase in the eastern equatorial Indian Ocean (EIO, Fig. 1) for the first time, detected using $p\text{CO}_2$ data collected during May 2012, together with historical data since 1962 as integrated by Takahashi et al. (2013) (i.e., LDEO_Database_V2012). We examine temporal changes in air–sea CO_2 flux and OA indicators (pH and aragonite saturation state, Ω_{arag}), and explore the factors responsible for the $p\text{CO}_2$ increase and OA.

2 Material and methods

2.1 Study site

The study region was located to the west of Sumatra, covering the area from 5° N to 5° S and 90 to 95° E (Fig. 1). The local climate is characterized by the seasonal monsoon, which exhibits a weak westerly annual mean wind and has a strong semiannual cycle. Consequently, the equatorial currents are quite unique and different from those in the other equatorial oceans (Schott et al., 2009). The ocean currents are mainly in the zonal direction and the most distinguished are the strong surface eastward flows, known as Wyrtki jets (Wyrtki, 1973), which occur during two intermonsoon periods in spring (April–May) and fall (October–November). There is no climatological equatorial upwelling due to lack of steady equatorial easterlies. Another important current is

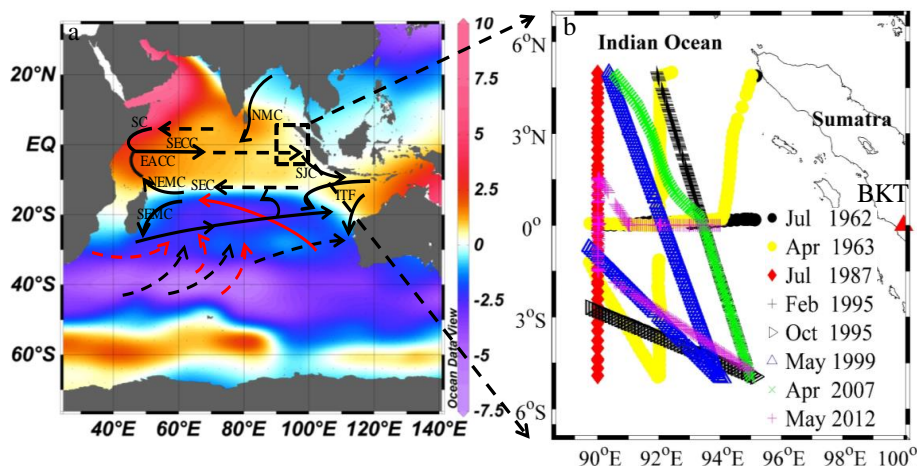


Figure 1. Study site (a) shows the relative location of the study site (within the dashed frame) in the Indian Ocean, annual air–sea CO_2 fluxes ($\text{mol C m}^{-2} \text{ yr}^{-1}$, colored) estimated by Takahashi et al. (2009), and schematic representations of ocean currents during the winter monsoon, redrawn from Schott et al. (2009). The currents shown in this map include the South Equatorial Current (SEC), South Equatorial Countercurrent (SECC), Northeast and Southeast Madagascar Current (NEMC and SEMC), East African Coastal Current (EACC), Somali Current (SC), Indonesian Throughflow (ITF), South Java Current (SJC), the Northeast Monsoon Current (NMC) during the winter monsoon, and so on. The subsurface return flow for the supergyre is shown in red. (b) shows the study site, the eastern equatorial Indian Ocean (EIO, $5^\circ \text{ N}–5^\circ \text{ S}$, $90^\circ–95^\circ \text{ E}$). The lines show all cruise tracks for surface CO_2 partial pressure ($p\text{CO}_2$) measurements during the 1962–2012 period in the EIO. The red triangle presents the location of the atmospheric CO_2 observation station in Bukit Kototabang, Indonesia (BKT, 0.20° S , 100.38° E).

the Equatorial Undercurrent (Knauss and Taft, 1964), which exists at the thermocline depth and occurs mainly during the later winter to spring. The strong equatorial zonal currents link the EIO with the western equatorial Indian Ocean, through which it joins the basin-scale circulation.

2.2 Data sources and processing

2.2.1 Data sources

Data in 2012 were from the Monsoon Onset Monitoring and its Social and Ecosystem Impact (MOMSEI) project cruise conducted during the period 1–9 May 2012. During this cruise, sea surface $p\text{CO}_2$ was continuously measured every 15 min with a HydroCTM CONTROS sensor. The CO_2 mole fraction in the headspace behind a membrane equilibrator was measured using a two-wavelength nondispersive infrared detector (NDIR). The equilibrator consists of a flat silicone composite membrane, and additional sensors for pressure, temperature, and relative humidity measurements. Regular zeroings are automatically performed to correct instrument drift with time by scrubbing CO_2 from the internal gas stream (Saderne et al., 2013). More details on $p\text{CO}_2$ measurements can be found in Saderne et al. (2013). Fietzek et al. (2013) presented the detailed in situ calibration of the data, and asserted that the average difference between sensor reading and reference $p\text{CO}_2$ was $-0.6 \pm 3.0 \mu\text{atm}$ with a root-mean-square error (RMSE) of $3.7 \mu\text{atm}$. Before the cruise in May 2012, a comparison study between this sen-

sor and the Apollo CO_2 instrument (e.g., Jiang et al., 2008) indicated an accuracy of better than $5 \mu\text{atm}$ (see Fig. s1 in the Supplement). During the MOMSEI cruise, sea surface temperature (SST) and salinity (SSS) data were also collected every 15 min using a SBE 21 Seacat thermosalinograph.

Surface water $p\text{CO}_2$ and its associated parameters (temperature and salinity) before 2012 were extracted from the Lamont-Doherty Earth Observatory (LDEO) Database (version V2012; Takahashi et al., 2013) (Tables 1 and 2). The $p\text{CO}_2$ results of the LDEO database are based on measurements made using air–seawater equilibration methods (Takahashi et al., 2013). All data points have been individually quality controlled before they were integrated into this database. The uncertainty of the $p\text{CO}_2$ data is estimated to be about $\pm 2.5 \mu\text{atm}$ on average, given differences in equilibrator designs, calibration methods, and some interpolated parameters (Takahashi et al., 2013).

In addition, several ancillary parameters including wind speed, atmospheric CO_2 concentration, mixed layer depth (MLD), SSS and chlorophyll *a* (Chl *a*) (Table 2) were used. Because long-term atmospheric CO_2 data since 1962 are not available in the Indian Ocean, we used atmospheric CO_2 data measured as the mole fraction in dry air at Mauna Loa, Hawaii (Table 2), as an alternative. Some limited observations collected during the 2004–2010 period at the BKT (Bukit Kototabang, Indonesia; Table 2) atmospheric CO_2 station, close to the study area (Fig. 1), showed that the atmospheric CO_2 level at Mauna Loa was at least 4.3 ppm larger than that at BKT, Indonesia (see Fig. s2). Therefore, we

Table 1. Summary of cruise information and mean values of surface temperature, salinity, and surface $p\text{CO}_2$ in the equatorial belt (2°N – 2°S , 90 – 95°E), which are reported as mean \pm standard deviation. These mean values in this table are calculated as described in Sect. 2.2.2, and are not deseasonalized.

Cruise name	Observation period ^a	Ship/experiment	Surface temperature	Surface salinity	Surface $p\text{CO}_2$
LUSIAD_62	30 Jun, 2–3 Jul 1962	R/V <i>Argo</i>	29.24 ± 0.21	34.21 ± 0.06^b	304 ± 2
LUSIAD_63	8–26 Apr 1963	R/V <i>Argo</i>	29.81 ± 0.26	33.84 ± 0.19^b	307 ± 4
SAGA_II_Leg_2	30 Jun–2 Jul 1987	R/V A. <i>Korolev SAGA II</i>	29.08 ± 0.19	34.47 ± 0.08	357 ± 9
R. F. Weiss Surface Data Files 42–63	10–17 Feb 1995	R/V <i>Knorr Weiss Data</i>	29.50 ± 0.24	33.74 ± 0.13^b	350 ± 2
IO95leg ^c	31 Oct–1 Nov 1995	R/V <i>M. Baldrige IO95</i>	29.19 ± 0.29	34.05 ± 0.31	359 ± 5
JASMINE1999_2	4–6, 28–31 May 1999	R/V <i>Ron Brown 1999</i>	29.34 ± 0.22	34.38 ± 0.19	373 ± 4
IO9N_Underway_ $p\text{CO}_2$	9–16 Apr 2007	CLIVAR repeat sections	29.83 ± 0.25	34.01 ± 0.05	381 ± 4
MOMSEI	1–9 May 2012	R/V <i>Madidihang 03</i>	30.00 ± 0.26	34.30 ± 0.08	385 ± 5

^a The observation period in this table refers to the period when the data used in this study were collected. ^b We used salinity data from the simple ocean data assimilation (SODA) since in situ data are not available during these cruises (http://coastwatch.pfeg.noaa.gov/erddap/griddap/hawaii_d90f_20ee_c4cb.graph). ^c We did not use data from this cruise to determine the trend due to the poor coverage latitudinally.

Table 2. Sources of data used in this study.

Parameter	Source
Sea surface salinity	SODA – POP 2.2.4 monthly means with a spatial resolution of $0.5^\circ \times 0.5^\circ$ (http://coastwatch.pfeg.noaa.gov/erddap/index.html)
Mixed layer depth ^a	IFREMER/LOS mixed layer depth climatology website with a spatial resolution of $2^\circ \times 2^\circ$ (www.ifremer.fr/cerweb/deboyer/mltd)
Chlorophyll <i>a</i>	SeaWiFS with a spatial resolution of $0.1^\circ \times 0.1^\circ$ (http://las.pfeg.noaa.gov/oceanWatch/oceanwatch.php)
Sea surface $p\text{CO}_2^b$	LDEO_Database_V2012, Takahashi et al. (2013) (http://cdiac.ornl.gov/ftp/oceans/LDEO_Database/Version_2012/)
Atmospheric CO_2	CO_2 monthly mean data from Mauna Loa, Hawaii, and Bukit Kototabang, Indonesia (BKT) (http://www.esrl.noaa.gov/gmd/ccgg/trends/mlo.html)
Wind speed	NCEP (National Centers for Environmental Prediction) wind speeds with a spatial resolution of $2.5^\circ \times 2.5^\circ$ (http://www.esrl.noaa.gov/psd/data/gridded/data.ncep.html)

^a This mixed layer depth is in fact a temperature–mixed layer depth, or isothermal layer depth. Mixed layer depths are computed as the depth with a 0.2°C absolute temperature difference from 10 m temperature (Keerthi et al., 2013). ^b See specific cruise information in Table 1.

corrected the atmospheric CO_2 concentration from Mauna Loa by subtracting 4.3 ppm. The atmospheric CO_2 mole fraction was then converted to $p\text{CO}_2$ by correcting to 100 % humidity at the mean SST and SSS during the investigation period, following Jiang et al. (2008).

2.2.2 Spatial averaging and seasonal correction

We first grouped all the data points (temperature, salinity, and $p\text{CO}_2$) into their individual 0.1° latitudinal bands, then calculated the average for each band, and took the average of all mean values from each band as cruise mean. Considering that very few of the cruises covered the entire study area well (Fig. 1), we just used the data in the equatorial belt (2°N – 2°S , 90 – 95°E) to determine the trends of SST, SSS, and $p\text{CO}_2$. We also corrected the effects of the seasonal cycle by using the climatological data from Takahashi et al. (2009) (Fig. s3) before the trend analysis.

2.3 Calculation of air–sea CO_2 fluxes

We calculated the air–sea CO_2 flux based on Eqs. (1) and (2):

$$F = 0.24 \times k \times s \times (p\text{CO}_2 \text{ water} - p\text{CO}_2 \text{ air}), \quad (1)$$

$$k = (0.262 \pm 0.022) \times U_{10}^2 \times (\text{Sc}/660)^{-0.5}, \quad (2)$$

where F is the air–sea CO_2 flux ($\text{mmol m}^{-2} \text{d}^{-1}$), in which a positive value represents CO_2 releasing from the ocean to the atmosphere; k is the gas transfer velocity (cm h^{-1}), calculated using Eq. (2) based on the parameterization of gas transfer velocity with wind speed proposed by Wanninkhof (1992) and recently revised by Ho et al. (2011); s is the solubility coefficient of CO_2 ($\text{mol L}^{-1} \text{atm}^{-1}$) (Weiss, 1974); and $p\text{CO}_2 \text{ water}$ and $p\text{CO}_2 \text{ air}$ are the $p\text{CO}_2$ in the surface ocean and in the atmosphere (μatm), respectively. In Eq. (2), U_{10} (m s^{-1}) is the wind speed at a height of 10 m above the sea surface. We used monthly mean wind speeds from the National Centers for Environmental Prediction

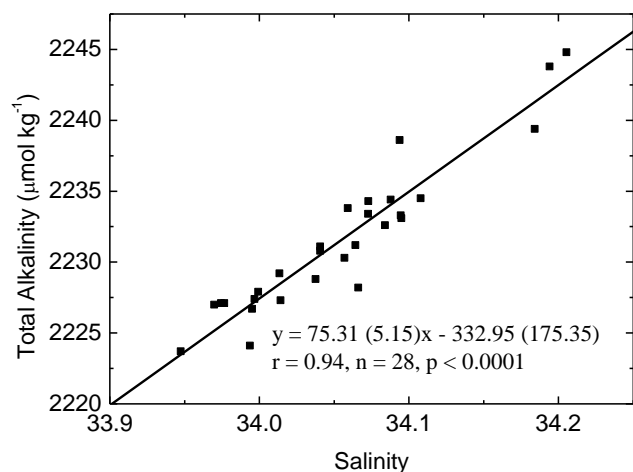


Figure 2. Relationship of total alkalinity (TA) and salinity determined from the upper 20 m data collected in April 2007 during the CLIVAR/ CO_2 section I9N cruise (<http://cchdo.ucsd.edu>).

(NCEP) with a spatial resolution of $2.5^\circ \times 2.5^\circ$ (<http://www.esrl.noaa.gov/psd/data/gridded/data.ncep.html>) for calculating of CO_2 fluxes. Sc is the Schmidt number, which was calculated based on the formula of Wanninkhof (1992).

2.4 Estimate of TA, DIC, pH and CaCO_3 saturation state

The conservative behavior of TA allows us to estimate TA using the salinity data collected. We used data in the upper 20 m collected in April 2007 in this region during the CLIVAR/ CO_2 (Climate Variability and Predictability) section I9N cruise (<http://cchdo.ucsd.edu>) to build the relationship between TA and SSS (Fig. 2) as follows:

$$\text{TA} = 75.31(\pm 5.15) \times \text{SSS} - 332.95(\pm 175.35) \quad (3)$$

($r = 0.94, n = 28, p < 0.0001$).

This relationship produces an RMSE of $1.7 \mu\text{mol kg}^{-1}$, which was less than that produced by the Lee et al. (2006) formula ($\pm 10.6 \mu\text{mol kg}^{-1}$).

The DIC (dissolved inorganic carbon), pH, and CaCO_3 saturation state were calculated from $p\text{CO}_2$, TA, temperature, and salinity using the CO2sys program (Lewis and Wallace, 1998) and adopting the CO_2 system coefficients of Mehrbach et al. (1973) as refitted by Dickson and Millero (1987). Because the saturation state of calcite is usually about 50 % greater than that of aragonite at 25°C (Mucci, 1983), hereafter we only discuss the results for Ω_{arag} .

2.5 Respective contribution of temperature, salinity, TA, and DIC to the changes of $p\text{CO}_2$, pH and Ω_{arag}

We used the method of Wakita et al. (2013) to quantify the contributions of temperature, salinity, TA, and DIC to

changes of $p\text{CO}_2$, pH, and Ω_{arag} . For example, the contributions of these properties to $p\text{CO}_2$ change can be expressed as the sum of the individual contributions as follows:

$$\Delta p\text{CO}_2 = (\alpha p\text{CO}_2/\alpha T)\Delta T + (\alpha p\text{CO}_2/\alpha S)\Delta S + (\alpha p\text{CO}_2/\alpha TA)\Delta TA + (\alpha p\text{CO}_2/\alpha \text{DIC})\Delta \text{DIC}, \quad (4)$$

where T and S are SST and SSS, respectively; and ΔT , ΔS , ΔDIC , and ΔTA denote the changes in SST, SSS, DIC, and TA, respectively.

During the calculation, we evaluated the rate of $p\text{CO}_2$ change by allowing one parameter to vary while using mean values for the other parameters. For example, we estimated the contribution of DIC change to $p\text{CO}_2$ ($(\alpha p\text{CO}_2/\alpha \text{DIC})\Delta \text{DIC}$) by calculating $p\text{CO}_2$ using the DIC trend from 1962 to 2012 and mean values for the other parameters, and then we computed the impact of DIC change on $p\text{CO}_2$. The contributions of these properties to pH and Ω_{arag} changes were calculated similarly.

3 Results and discussion

3.1 Temporal change of surface water $p\text{CO}_2$

The in situ sea surface $p\text{CO}_2$ data in the EIO starting from 1962 are shown in Figs. 3 and 4. Spatially, $p\text{CO}_2$ distributions were relatively homogeneous in each cruise, with a standard deviation of less than $9 \mu\text{atm}$ (Fig. 3). A gradual increase in sea surface $p\text{CO}_2$ with time is the most evident feature (Figs. 3, 4). The mean value of sea surface $p\text{CO}_2$ in the equatorial belt (2°N – 2°S , 90 – 95°E) increased from $\sim 307 \mu\text{atm}$ in April 1963 to $\sim 373 \mu\text{atm}$ in May 1999, $\sim 381 \mu\text{atm}$ in April 2007, and $\sim 385 \mu\text{atm}$ in May 2012 (Fig. 4, Table 1). After seasonal correction, we find that sea surface $p\text{CO}_2$ increased at a mean rate of $1.56 \pm 0.08 \mu\text{atm yr}^{-1}$ from 1963 to 2012 (Fig. 4a).

For comparison purposes, we also estimated the surface $p\text{CO}_2$ trend along the Equator from 89.5 to 94.5°E , and found that since the International Indian Ocean Expedition (IIOE, 1960–1965), surface $p\text{CO}_2$ increased from $307 \pm 4 \mu\text{atm}$ in April 1963 to $392 \pm 6 \mu\text{atm}$ in May 2012 (Fig. 4b), with a mean rate of $\sim 1.64 \mu\text{atm yr}^{-1}$ (after seasonal correction). This rate of surface $p\text{CO}_2$ increase is not significantly different from that obtained using all data measured during the 1962–2012 period (Fig. 4a). The $p\text{CO}_2$ increase rate in the EIO is similar to that in the subtropical North Atlantic (Bates, 2007), higher than that in the western tropical North Atlantic (Park and Wanninkhof, 2012), and lower than that in the equatorial Atlantic and Pacific (Oudot et al., 1995; Takahashi et al., 2006) (Table 3).

3.2 Temporal changes of air–sea CO_2 flux, pH, and Ω_{arag}

The increase in surface $p\text{CO}_2$ could potentially affect air–sea CO_2 flux by changing the gradient of air–sea $p\text{CO}_2$ (Eq. 1).

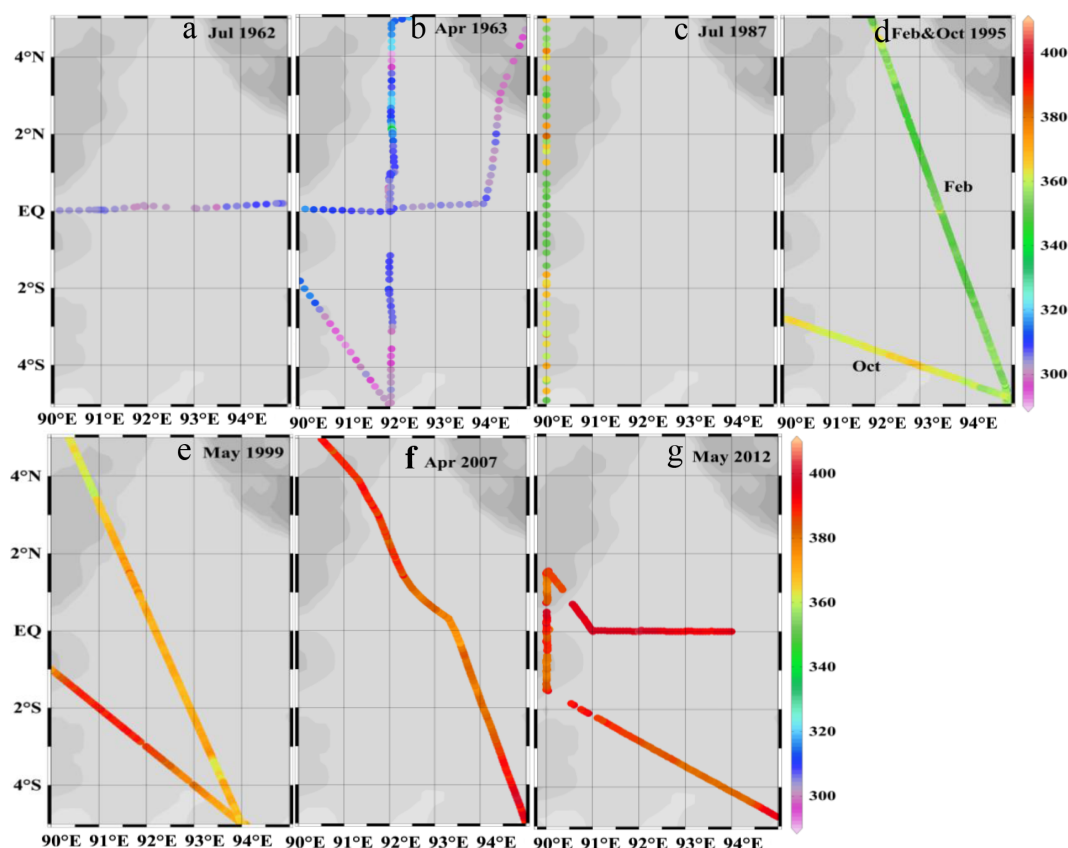


Figure 3. Sea surface CO_2 partial pressure ($p\text{CO}_2$) observed in July 1962 (a), April 1963 (b), July 1987 (c), February and October 1995 (d), May 1999 (e), April 2007 (f), and May 2012 (g) in the EIO. This figure is plotted with ODV software (Schlitzer, 2014).

Table 3. Sea surface $p\text{CO}_2$ trend observed in various regions of the ocean.

Region	Period	$p\text{CO}_2$ growth rate ($\mu\text{atm yr}^{-1}$)	Sink/source ^a	Reference
Eastern subpolar Atlantic (32–10° W, 50–64° N)	1972–1989	2.3 (± 0.8)	sink	Omar and Olsen (2006)
Subtropical North Atlantic near Bermuda	1983–2003	1.7 (± 0.3)	sink	Bates (2007)
Western tropical North Atlantic	2002–2009	1.01–1.11	sink	Park and Wanninkhof (2012)
Eastern equatorial Atlantic	1982–1992 ^b	2.5–2.8	source	Oudot et al. (1995)
Subarctic western North Pacific	1995–2003	1.6 (± 1.7)	sink	Lenton et al. (2012)
Western subtropical North Pacific	1995–2005	1.8 (± 0.6)	sink	Lenton et al. (2012)
Eq. Pacific (Niño 3.4 and warm pool regions included)	1990–2004	1.8–2.3	source	Takahashi et al. (2006)
East eq. Indian Ocean (90–100° E, 2° S–2° N, spring)	1963–2012	1.56 (± 0.08)	source	this study
Southwestern Indian Ocean (30–90° E, 50–55° S, summer)	1991–2007	2.4 (± 0.2)	sink	Metzl (2009)
Indian and Pacific sectors of the Southern Ocean	1995–2008	2.2 (± 0.2)	sink	Lenton et al. (2012)

^a “sink” means that the ocean absorbs atmospheric CO_2 , while “source” indicates that the ocean releases CO_2 to the atmosphere. ^b The growth rate here refers to the mean difference between 1982 and 1992.

The mean rate of $p\text{CO}_2$ increase in the EIO from 1962 to 2012 ($\sim 1.56 \mu\text{atm yr}^{-1}$) was only slightly greater than that in the atmosphere ($\sim 1.46 \mu\text{atm yr}^{-1}$; Fig. 4a), suggesting a weak trend of increase for the air–sea CO_2 gradient (Fig. 5a). Equation (1) showed that the air–sea CO_2 flux could also be affected by the gas transfer velocity, which is typically expressed as a power function of wind speed (e.g., Wanninkhof,

1992). Figure 5 showed no obvious changes in wind speed. All factors considered, air–sea CO_2 fluxes showed a weak but insignificant increasing trend during the 1962–2012 period (Fig. 5).

OA has taken place in this region during the past 50 yr, as indicated by pH and Ω_{arag} . Surface water pH (in the total hydrogen scale) decreased significantly at a rate of

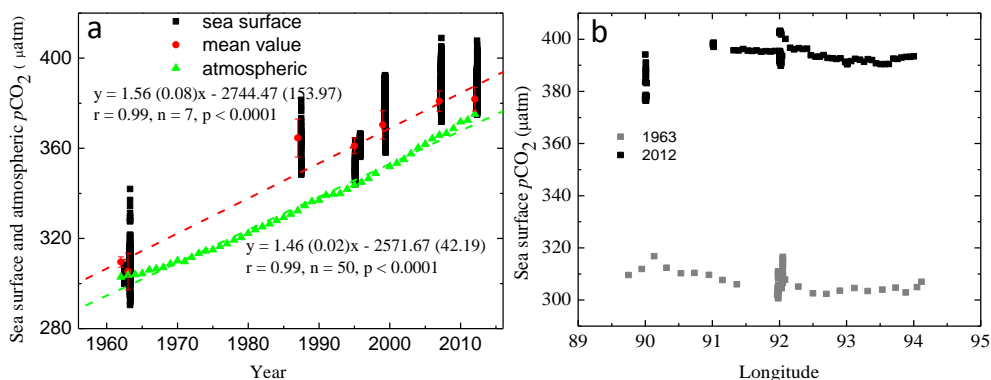


Figure 4. Temporal changes in sea surface $p\text{CO}_2$ (black squares) and atmospheric $p\text{CO}_2$ (green triangles) measured at Mauna Loa, Hawaii (a), and sea surface $p\text{CO}_2$ along the Equator during April 1963 and May 2012 (b). The dashed line in (a) shows the linear regression line based on the mean value of each cruise (red circle), which has been deseasonalized using the climatological data identified by Takahashi et al. (2009).

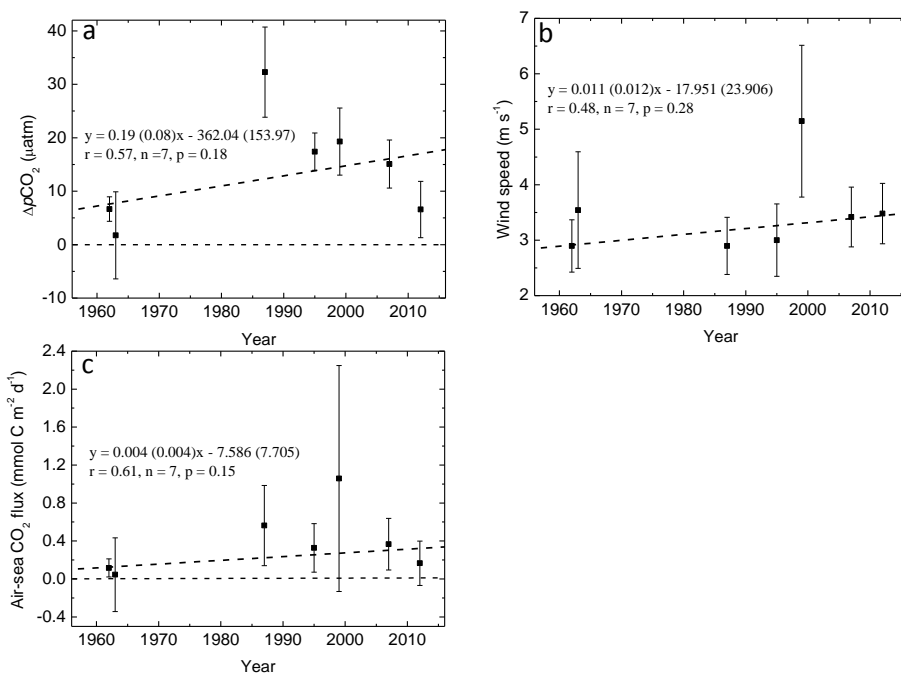


Figure 5. Temporal changes in the difference of $p\text{CO}_2$ between the atmosphere and the ocean ($\Delta p\text{CO}_2 = p\text{CO}_2_{\text{water}} - p\text{CO}_2_{\text{air}}$) (a), wind speed (b), and air–sea CO_2 flux (c). All data are corrected to the same month (April).

$-0.0016 \pm 0.0001 \text{ yr}^{-1}$ from 1962 to 2012 (Fig. 6), similar to the rate observed at the time-series stations of Bermuda (BATS) and Hawaii (HOT) (Takahashi and Sutherland, 2013). An average decline of 0.08 pH units over the past 50 yr (1963–2012) in the EIO is surprising, considering that the average surface ocean pH has just declined by about 0.1 units since the 1700s due to the absorption of anthropogenic CO_2 (Raven et al., 2005). A rapid reduction in Ω_{arag} with a rate of $-0.0095 \pm 0.0005 \text{ yr}^{-1}$ in this region was also observed (Fig. 6). This reduction rate is faster than that in the subsurface waters in the subarctic western North Pa-

cific Ocean (-0.004 to -0.005 yr^{-1}) (Wakita et al., 2013), and similar to that in the southern California Current system ($0.009 \pm 0.006 \text{ yr}^{-1}$) (Leinweber and Gruber, 2013) and in the North Atlantic Ocean ($-0.0100 \pm 0.0012 \text{ yr}^{-1}$) (Bates et al., 2012).

3.3 Contributions of temperature, salinity, TA, and DIC changes to the increase in $p\text{CO}_2$, and decreases in pH and Ω_{arag}

Using the method of Wakita et al. (2013), we quantified the contribution of temperature, salinity, TA, and DIC (Fig. 7) to

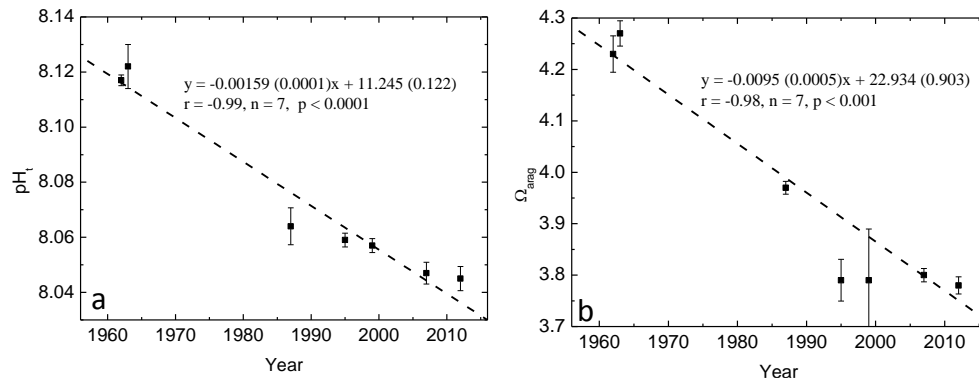


Figure 6. Temporal changes in sea surface pH (in the total hydrogen scale, pH_T) (a) and aragonite saturation state (Ω_{arag}) (b). pH_T and Ω_{arag} were calculated from $p\text{CO}_2$ and TA as described in Sect. 2.4. All data are corrected to the same month (April).

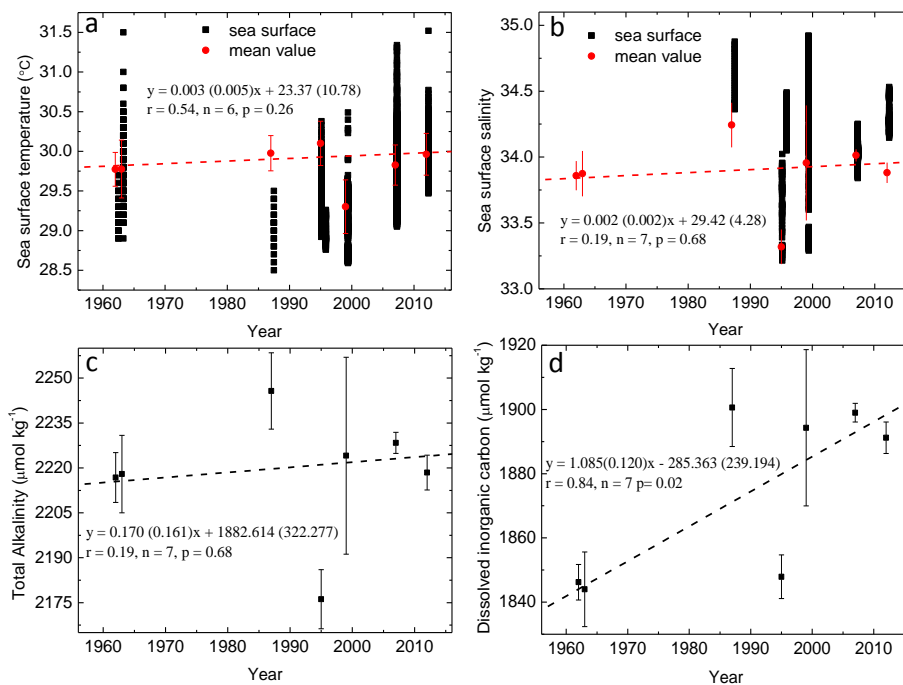


Figure 7. Temporal changes in sea surface temperature (a), salinity (b), TA (c), and DIC (d). TA was estimated from SSS, and DIC was calculated from $p\text{CO}_2$ and TA as described in Sect. 2.4. All data are corrected to the same month (April).

the increase in surface $p\text{CO}_2$ and decreases in pH and Ω_{arag} . The results show that the DIC increase played the most important role in elevating surface water $p\text{CO}_2$ and decreasing pH and Ω_{arag} . In contrast, the contributions from temperature, salinity, and TA were insignificant (Fig. 8). These results (Fig. 8) are in good agreement with the trends of temperature, salinity, TA, and DIC (Fig. 7). From 1962 to 2012, the changes of temperature, salinity, and TA were not significant, while DIC increased significantly during the 1962–2012 period (Fig. 7). In addition, the good consistency between the sum of the decomposed individual contributions (Tot) and the observed trend (Obs) verified the robustness of the method of Wakita et al. (2013) in our study (Fig. 8).

3.4 Factors contributing to the DIC increase

3.4.1 Air–sea CO_2 exchange

It is obvious that the DIC increase with time was not due to local uptake of CO_2 via air–sea exchange, given that the EIO was almost always a CO_2 source to the atmosphere (Fig. 5, Bates et al., 2006; Takahashi et al., 2009). However, the rapidly rising atmospheric CO_2 since 1962 created the potential to reduce or even reverse the CO_2 release in this region from the ocean to the atmosphere (Fig. 4), and can directly induce DIC increase in the mixed layer. Figure 9 gives a schematic of DIC increase in the mixed layer induced by

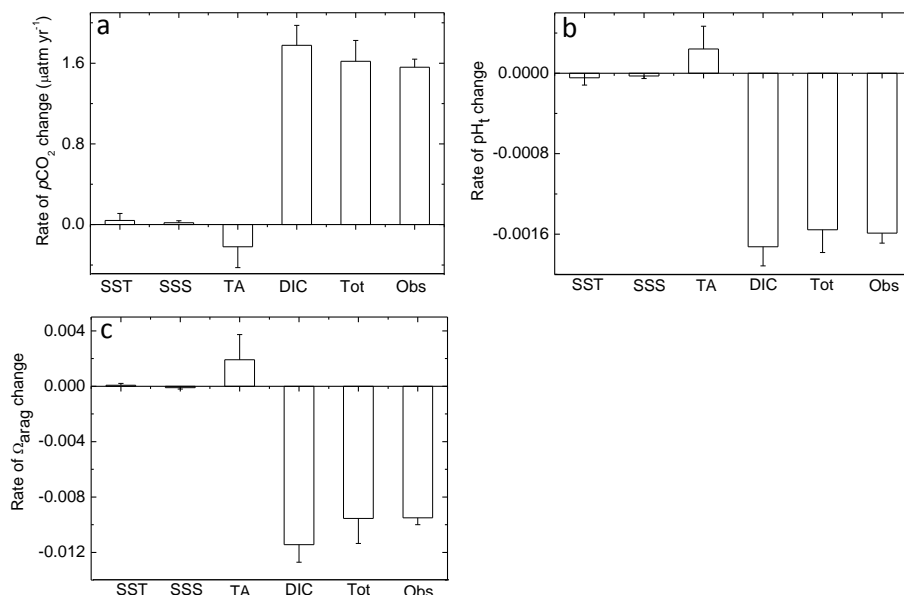


Figure 8. Contribution of SST, SSS, TA and DIC to the change of $p\text{CO}_2$ (a), pH_t (b), and aragonite saturation state, Ω_{arag} (c). Tot denotes the sum of the decomposed individual contributions and Obs the observed trend.

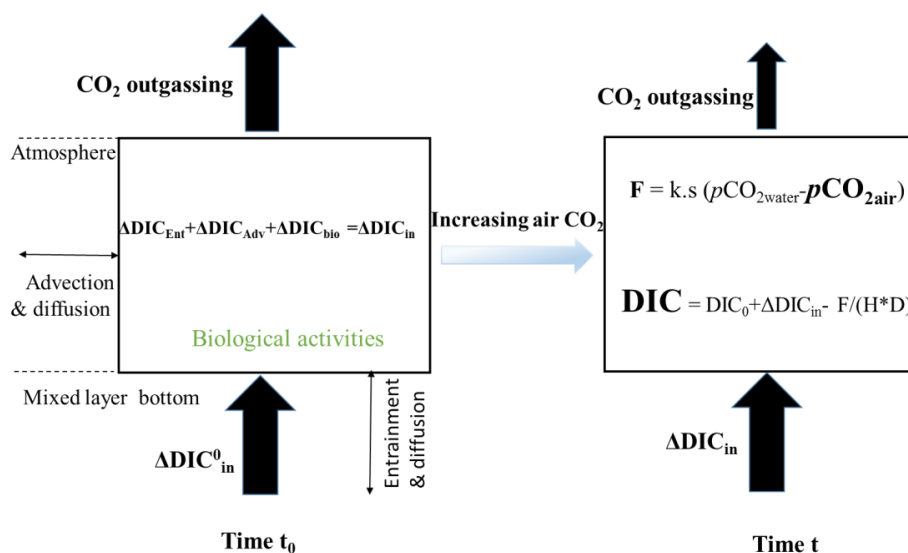


Figure 9. A schematic of DIC increase in the mixed layer induced by atmospheric CO_2 increase in a CO_2 source region with respect to the atmosphere. DIC changes in the mixed layer can be attributed to vertical entrainment ($\Delta\text{DIC}_{\text{Ent}}$), vertical and horizontal advection and diffusion ($\Delta\text{DIC}_{\text{Adv}}$), biological activities ($\Delta\text{DIC}_{\text{bio}}$) and air–sea exchange ($\Delta\text{DIC}_{\text{as}}$). From time t_0 to t when atmospheric CO_2 increases, the driving force of air–sea exchange ($p\text{CO}_{2\text{ water}} - p\text{CO}_{2\text{ air}}$) and correspondingly the CO_2 outgassing from the ocean to the atmosphere would decrease. This may induce DIC increase in the mixed layer due to reduction in the magnitude of CO_2 source (Schneider et al., 2012). F denotes air–sea CO_2 fluxes, k the gas transfer velocity, s the solubility coefficient of CO_2 , and $p\text{CO}_{2\text{ water}}$ and $p\text{CO}_{2\text{ air}}$ are the $p\text{CO}_2$ in the surface ocean and in the atmosphere. Details on air–sea CO_2 fluxes can be found in Sect. 2.3. H and D are mixed layer depth and seawater density, respectively.

atmospheric CO_2 increase in a CO_2 source region with respect to the atmosphere. When atmospheric CO_2 concentration increases, CO_2 outgassing in this region from the ocean to the atmosphere would be reduced or even reversed, and would increase DIC concentration in the mixed layer. Thus,

oceanic DIC increase in a CO_2 source region to the atmosphere could be caused via reduction in the magnitude of CO_2 source (Schneider et al., 2012), different from the situation in a CO_2 sink region, where more anthropogenic CO_2

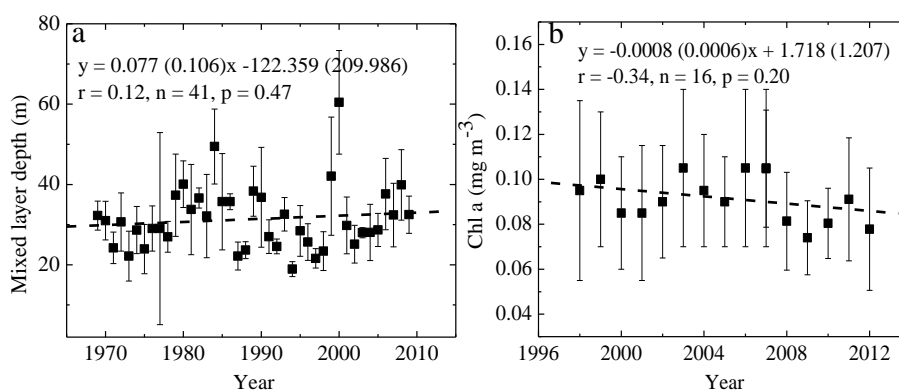


Figure 10. Temporal changes in mixed layer depth (a), and Chl *a* (b). Squares show the mean value, and bars show the standard deviation. See Table 2 for more details on data sources. All data are from the same month (April).

was directly absorbed by the ocean from the atmosphere due to higher atmospheric CO_2 concentrations.

3.4.2 Ocean circulation

Transport via basin-scale ocean circulation also contributed to DIC increase. This can be verified by the high contents of anthropogenic CO_2 in the mixed layer of the EIO (e.g., Sabine et al., 1999; Sabine et al., 2004), which has no direct uptake of atmospheric CO_2 (Fig. 5, Bates et al., 2006; Takahashi et al., 2009). The observed increase in anthropogenic CO_2 in the EIO is likely due to accumulation of anthropogenic CO_2 in CO_2 sink regions and subsequent transport to the equatorial belt via basin-scale ocean circulation. For instance, carbon in the region between 15 and 50° S in the Indian Ocean could be finally transported to the EIO. On the one hand, this region (between 15 and 50° S) is a major subduction zone (Schott et al., 2009), serves as a significant sink of atmospheric CO_2 (Fig. 1a, Takahashi et al., 2009; Valsala et al., 2012), and hosts the largest inventories of anthropogenic CO_2 across the Indian Ocean (Sabine et al., 2004). Furthermore, it is reported that the oceanic increase in carbon storage roughly kept pace with atmospheric CO_2 increase (Sabine et al., 1999).

On the other hand, the upper ocean horizontal circulation and the meridional overturning cells are believed to account for carbon transport towards the EIO (Fig. 1; Schott et al., 2002; Schott et al., 2009; Valsala et al., 2012). In the upper layer, water masses move westward in the South Equatorial Current (SEC) and partly merge into the East African Coast Current (EACC); they can move further to the EIO along with the eastward flows, including the South Equatorial Countercurrent (SECC), the Wyrki jets (Wyrki, 1973), and the Equatorial Undercurrent (EUC) (Knauss and Taft, 1964). At the thermocline depth, shallow overturning cells, including the cross-equatorial cell (CEC) and the Southern Hemisphere subtropical cell (STC), bring water masses from the subduction zone to the off-equatorial upwelling zone, where

they upwell to the surface. Thus, the southern subtropical Indian Ocean may act as a window for carbon uptake (Valsala et al., 2012), and the basin-scale circulation provides the route to transport the absorbed anthropogenic CO_2 ultimately to the EIO. A similar mechanism was also proposed in the equatorial Pacific by Feely et al. (1999), who pointed out that entrained subtropical water was injected into upwelled water at the Equator.

Nevertheless, the pathways of ocean circulation are very complicated, and there must be other ways to increase DIC in the equatorial Indian Ocean. For instance, the Red Sea–Persian Gulf Intermediate Waters formed in the northwestern Indian Ocean carry anthropogenic CO_2 signals and spread equatorward (Sabine et al., 2004; Alvarez et al., 2009, and references therein), which also contributes to the increase of equatorial waters' DIC. Overall, ocean circulation may play an important role in transporting carbon accumulated in the CO_2 sink region to the equatorial belt on a basin scale. To a large extent, this could account for the paradox that the increase in anthropogenic CO_2 occurred in the CO_2 source region, where CO_2 was emitted to the atmosphere from the ocean.

3.4.3 Vertical mixing and biological activity

Vertical mixing with deep waters rich in CO_2 can elevate surface DIC content. For instance, the enhanced vertical mixing, usually accompanied by salinity rise and MLD deepening, will bring more CO_2 -rich waters to the surface layer, leading to higher DIC levels (e.g., Takahashi et al., 2006; Dumousseaud et al., 2010). However, there was no significant trend for SSS and MLD during the study period (Figs. 7, 10), indicating an insignificant influence of vertical mixing on DIC changes.

Biological activity could also affect DIC (e.g., Zhang et al., 2010). Model studies indicate that there were no significant changes in net primary production, particle export and export efficiency from 1960 to 2006 in this region (Laufkötter et al.,

2013). Satellite data also do not show a significant trend for Chl *a* (a proxy for biological activity) from 1998 to 2012 (Fig. 10). Therefore, biological activity was not the main factor leading to DIC rise, either.

4 Summary and conclusions

We compiled sea surface $p\text{CO}_2$ data in the eastern equatorial Indian Ocean over the past 50 yr to document the long-term trends in the inorganic carbon system. Results show that sea surface $p\text{CO}_2$ in the EIO increased significantly from 1962 to 2012. The mean rate of oceanic $p\text{CO}_2$ increase ($\sim 1.56 \mu\text{atm yr}^{-1}$) was close to the rate of atmospheric CO_2 increase ($\sim 1.46 \mu\text{atm yr}^{-1}$). Despite the steady $p\text{CO}_2$ increase in this region, no significant change in air–sea CO_2 fluxes during this period is detected. Ocean acidification as indicated by pH and Ω_{arag} did take place during this study period. Surface pH (total hydrogen scale) and Ω_{arag} decreased significantly at rates of -0.0016 ± 0.0001 and $-0.0095 \pm 0.0005 \text{ yr}^{-1}$, respectively. The increase in DIC is the main driver contributing to the increase in surface $p\text{CO}_2$ and decreases in pH and Ω_{arag} . The increase in DIC was most likely associated with the increasing atmospheric CO_2 concentration, and the transport of accumulated anthropogenic CO_2 from a CO_2 sink region via basin-scale ocean circulations. These two processes may combine to drive oceanic DIC to follow atmospheric CO_2 increase.

This study improved the understanding of the temporal changes of the inorganic carbon system in the Indian Ocean, demonstrating that big changes in carbon chemistry (e.g., OA) and other marine biogeochemical processes may have taken place in the Indian Ocean since the IIOE. However, the influences of climate events on oceanic $p\text{CO}_2$ and hence the oceanic carbon sink were not taken into account, due to spatial heterogeneity and scarcity of data. Long-term and continuous CO_2 observations with good resolutions are needed in the future in the Indian Ocean, where climate events such as the Indian Ocean Dipole (IOD) and El Niño–Southern Oscillation (ENSO) often occur (e.g., Currie et al., 2013; Valsala and Maksyutov, 2013).

The Supplement related to this article is available online at doi:10.5194/bg-11-6293-2014-supplement.

Acknowledgements. This work was funded by the Monsoon Onset Monitoring and its Social and Ecosystem Impact (MOMSEI) program (GY07–13), the FIO basic science and research programs (GY02–2012T03 and GY02–2007T08), and the Ocean Acidification program (DC0314031). We thank Frank Millero for providing the total alkalinity data. Great thanks are given to Wei-Jun Cai for his useful suggestions. We also thank Sarah R. Cooley from the Woods Hole Oceanographic Institution for her help in polishing

the language. Special thanks are given to the editor and the two anonymous reviewers for their useful comments and constructive suggestions.

Edited by: R. Hood

References

- Allen, G. R. and Adrim, M.: Coral reef fishes of Indonesia, *Zool. Stud.*, 42, 1–72, 2003.
- Álvarez, M., Lo Monaco, C., Tanhua, T., Yool, A., Oschlies, A., Bullister, J. L., Goyet, C., Metzl, N., Touratier, F., McDonagh, E., and Bryden, H. L.: Estimating the storage of anthropogenic carbon in the subtropical Indian Ocean: a comparison of five different approaches, *Biogeosciences*, 6, 681–703, doi:10.5194/bg-6-681-2009, 2009.
- Bates, N. R.: Interannual variability of the oceanic CO_2 sink in the subtropical gyre of the North Atlantic Ocean over the last 2 decades, *J. Geophys. Res.*, 112, C09013, doi:10.1029/2006JC003759, 2007.
- Bates, N. R., Pequignet, A. C., and Sabine, C. L.: Ocean carbon cycling in the Indian Ocean: 1. Spatiotemporal variability of inorganic carbon and air–sea CO_2 gas exchange, *Global Biogeochem. Cy.*, 20, GB3020, 2006.
- Bates, N. R., Best, M. H. P., Neely, K., Garley, R., Dickson, A. G., and Johnson, R. J.: Detecting anthropogenic carbon dioxide uptake and ocean acidification in the North Atlantic Ocean, *Biogeosciences*, 9, 2509–2522, doi:10.5194/bg-9-2509-2012, 2012.
- Caldeira, K. and Wickett, M. E.: Anthropogenic carbon and ocean pH, *Nature*, 425, p. 365, 2003.
- Currie, J. C., Lengaigne, M., Vialard, J., Kaplan, D. M., Aumont, O., Naqvi, S. W. A., and Maury, O.: Indian Ocean Dipole and El Niño/Southern Oscillation impacts on regional chlorophyll anomalies in the Indian Ocean, *Biogeosciences*, 10, 6677–6698, doi:10.5194/bg-10-6677-2013, 2013.
- Dickson, A. G. and Millero, F. J.: A comparison of the equilibrium constants for the dissociation of carbonic acid in seawater media, *Deep-Sea Res. A*, 34, 1733–1743, 1987.
- Doney, S. C., Fabry, V. J., Feely, R. A., and Kleypas, J. A.: Ocean Acidification: The other CO_2 problem, *Annu. Rev. Mar. Sci.*, 1, 169–192, 2009.
- Dumousseaud, C., Achterberg, E. P., Tyrrell, T., Charalampopoulou, A., Schuster, U., Hartman, M., and Hydes, D. J.: Contrasting effects of temperature and winter mixing on the seasonal and inter-annual variability of the carbonate system in the Northeast Atlantic Ocean, *Biogeosciences*, 7, 1481–1492, doi:10.5194/bg-7-1481-2010, 2010.
- Fay, A. R. and McKinley, G. A.: Global trends in surface ocean $p\text{CO}_2$ from in situ data, *Global Biogeochem. Cy.* 27, 1–17, 2013.
- Feely, R. A., Wanninkhof, R., Takahashi, T., and Tans, P.: Influence of El Niño on the equatorial Pacific contribution to atmospheric CO_2 accumulation, *Nature*, 398, 597–601, 1999.
- Feely, R. A., Sabine, C. L., Lee, K., Berelson, W., Kleypas, J., Fabry, V. J., and Millero, F. J.: Impact of Anthropogenic CO_2 on the CaCO_3 System in the Oceans, *Science*, 305, 362–366, 2004.
- Fietzek, P., Fiedler, B., Steinhoff, T., and Körtzinger, A.: In situ quality assessment of a novel underwater $p\text{CO}_2$ sensor based on membrane equilibration and NDIR spectrometry, *J. Atmos. Ocean Tech.*, 31, 181–196, 2013.

- Ho, D. T., Wanninkhof, R., Schlosser, P., Ullman, D. S., Hebert, D., and Sullivan, K. F.: Toward a universal relationship between wind speed and gas exchange: Gas transfer velocities measured with $3\text{He}/\text{SF}_6$ during the Southern Ocean Gas Exchange Experiment, *J. Geophys. Res.*, 116, C00F04, 2011.
- Jiang, L.-Q., Cai, W.-J., Wanninkhof, R., Wang, Y., and Lüger, H.: Air-sea CO_2 fluxes on the US South Atlantic Bight: Spatial and seasonal variability, *J. Geophys. Res.*, 113, C07019, doi:10.1029/2007JC004366, 2008.
- Keerthi, M. G., Lengaigne, M., Vialard, J., de Boyer Montégut, C., and Muraleedharan, P. M.: Interannual variability of the Tropical Indian Ocean mixed layer depth, *Ocean Dynam.*, 40, 743–759, 2013.
- Knauss, J. A. and Taft, B. A.: Equatorial Undercurrent of the Indian Ocean, *Science*, 143, 354–356, 1964.
- Laufkötter, C., Vogt, M., and Gruber, N.: Long-term trends in ocean plankton production and particle export between 1960–2006, *Biogeosciences*, 10, 7373–7393, doi:10.5194/bg-10-7373-2013, 2013.
- Lee, K., Tong, L. T., Millero, F. J., Sabine, C. L., Dickson, A. G., Goyet, C., Park, G., Wanninkhof, R., Feely, R. A., and Key, R. M.: Global relationships of total alkalinity with salinity and temperature in surface waters of the world's oceans, *Geophys. Res. Lett.*, 33, L19605, doi:10.1029/2006GL027207, 2006.
- Lefèvre, N., Watson, A. J., Olsen, A., Ríos, A. F., Pérez, F. F., and Johannessen, T.: A decrease in the sink for atmospheric CO_2 in the North Atlantic, *Geophys. Res. Lett.*, 31, L07306, doi:10.1029/2003GL018957, 2004.
- Leinweber, A. and Gruber, N.: Variability and trends of ocean acidification in the Southern California Current System: A timeseries from Santa Monica Bay. *J. Geophys. Res.*, 118, 3622–3633, 2013.
- Lenton, A., Metzl, N., Takahashi, T., Kuchinke, M., Matear, R. J., Roy, T., Sutherland, S. C., Sweeney, C., and Tilbrook, B.: The observed evolution of oceanic $p\text{CO}_2$ and its drivers over the last two decades, *Global Biogeochem. Cy.*, 26, GB2021, doi:10.1029/2011GB004095, 2012.
- Le Quééré, C., Raupach, M. R., Canadell, J. G., Marland, G., Bopp, L., Ciais, P., Conway, T., Doney, S., Feely, R., Foster, P., Friedlingstein, P., Gurney, K., Houghton, R. A., House, J. I., Huntingford, C., Levy, P. E., Lomas, M. R., Majkut, J., Metzl, N., Ometto, J. P., Peters, G. P., Prentice, I. C., Randerson, J. T., Running, S., Sarmiento, J. L., Schuster, U., Sitch, S., Takahashi, T., Viovy, N., van der Werf, G. R., and Woodward, F. L.: Trends in the sources and sinks of carbon dioxide, *Nat. Geosci.*, 2, 831–836, 2009.
- Le Quééré, C., Peters, G. P., Andres, R. J., Andrew, R. M., Boden, T. A., Ciais, P., Friedlingstein, P., Houghton, R. A., Marland, G., Moriarty, R., Sitch, S., Tans, P., Arneeth, A., Arvanitis, A., Bakker, D. C. E., Bopp, L., Canadell, J. G., Chini, L. P., Doney, S. C., Harper, A., Harris, I., House, J. I., Jain, A. K., Jones, S. D., Kato, E., Keeling, R. F., Klein Goldewijk, K., Ortzinger, K., A., Koven, C., Lef Evre, N., Maignan, F., Omar, A., Ono, T., Park, G. H., Pfeil, B., Poulter, B., Raupach, M. R., Regnier, P., Odenbeck, R., C., Saito, S., Schwinger, J., Segsneider, J., Stocker, B. D., Takahashi, T., Tilbrook, B., van Heuven, S., Viovy, N., Wanninkhof, R., Wiltshire, A., and Zaehle, S.: Global carbon budget 2013, *Earth Syst. Sci. Data*, 6, 235–263, doi:10.5194/essd-6-235-2014, 2014.
- Lewis, E. and Wallace, D. W. R.: Program developed for CO_2 systems calculations, ORNL/CDIAC 105, Carbon Dioxide Information Analysis Center, Oak Ridge National Laboratory US Department of Energy, Oak Ridge, Tennessee, 1998.
- Mehrbach, C., Culbertson, C. H., Hawley, J. E., and Pytkowicz, R. M.: Measurement of the Apparent Dissociation Constants of Carbonic Acid in Seawater at Atmospheric Pressure, *Limnol. Oceanogr.*, 18, 897–907, 1973.
- Metzl, N.: Decadal increase of oceanic carbon dioxide in Southern Indian Ocean surface waters (1991–2007), *Deep-Sea Res. II*, 56, 607–619, 2009.
- Mucci, A.: The solubility of calcite and aragonite in seawater at various salinities, temperatures, and one atmosphere total pressure, *Am. J. Sci.*, 283, 780–799, 1983.
- Naqvi, S.: Air-sea interactions and exchanges, in: Report of the Indian Ocean Synthesis Group on the Arabian Sea process study, edited by: Watts, L., Burkill, P., and Smith, S., JGOFS International Project Office, University of Bergen, Norway, 13–23, 2002.
- Omar, A. M. and Olsen, A.: Reconstructing the time history of the air-sea CO_2 disequilibrium and its rate of change in the eastern subpolar North Atlantic, 1972–1989, *Geophys. Res. Lett.*, 33, L04602, doi:10.1029/2005GL025425, 2006.
- Orr, J. C., Fabry, V. J., Aumont, O., Bopp, L., Doney, S. C., Feely, R. A., Gnanadesikan, A., Gruber, N., Ishida, A., Joos, F., Key, R. M., Lindsay, K., Maier-Reimer, E., Matear, R., Monfray, P., Mouchet, A., Najjar, R. G., Plattner, G., Rodgers, K. B., Sabine, C. L., Sarmiento, J. L., Schlitzer, R., Slater, R. D., Totterdell, I. J., Weirig, M., Yamanaka, Y., and Yool, A.: Anthropogenic ocean acidification over the twenty-first century and its impact on calcifying organisms, *Nature*, 437, 681–686, 2005.
- Oudot, C., TERNON, J., and Lecomte, J.: Measurements of atmospheric and oceanic CO_2 in the tropical Atlantic: 10 years after the 1982–1984 FOCAL cruises, *Tellus B*, 47, 70–85, 1995.
- Park, G. and Wanninkhof, R.: A large increase of the CO_2 sink in the western tropical North Atlantic from 2002 to 2009, *J. Geophys. Res.*, 117, C8029, doi:10.1029/2011JC007803, 2012.
- Raven, J., Caldeira, K., Elderfield, H., Hoegh-Guldberg, O., Liss, P., Riebesell, U., Shepherd, J., Turley, C., and Watson, A.: Ocean acidification due to increasing atmospheric carbon dioxide, *The Royal Society, London*, 1–60, 2005.
- Sabine, C. L., Key, R. M., Johnson, K. M., Millero, F. J., Poisson, A., Sarmiento, J. L., Wallace, D. W. R., and Winn, C. D.: Anthropogenic CO_2 inventory of the Indian Ocean, *Global Biogeochem. Cy.*, 13, 179–198, 1999.
- Sabine, C. L., Key, R. M., Feely, R. A., and Greeley, D.: Inorganic carbon in the Indian Ocean: Distribution and dissolution processes, *Global Biogeochem. Cy.*, 16, 10–1029, 2002.
- Sabine, C. L., Feely, R. A., Gruber, N., Key, R. M., Lee, K., Bullister, J. L., Wanninkhof, R., Wong, C. S., Wallace, D. W. R., Tilbrook, B., Millero, F. J., Peng, T. H., Kozyr, A., Ono, T., and Rios, A. F.: The Oceanic Sink for Anthropogenic CO_2 , *Science*, 305, 367–371, 2004.
- Saderne, V., Fietzek, P., and Herman, P. M. J.: Extreme Variations of $p\text{CO}_2$ and pH in a Macrophyte Meadow of the Baltic Sea in Summer: Evidence of the Effect of Photosynthesis and Local Upwelling, *PLoS ONE*, 8, e62689, doi:10.1371/journal.pone.0062689, 2013.

- Sarma, V. V. S. S., Lenton, A., Law, R. M., Metzl, N., Patra, P. K., Doney, S., Lima, I. D., Dlugokencky, E., Ramonet, M., and Valsala, V.: Sea-air CO_2 fluxes in the Indian Ocean between 1990 and 2009, *Biogeosciences*, 10, 7035–7052, doi:10.5194/bg-10-7035-2013, 2013.
- Schlitzer, R.: Ocean Data View, <http://odv.awi.de>, 2014.
- Schneider, A., Tanhua, T., Körtzinger, A., and Wallace, D. W. R.: An evaluation of tracer fields and anthropogenic carbon in the equatorial and the tropical North Atlantic, *Deep-Sea Res. I*, 67, 85–97, 2012.
- Schott, F. A. and McCreary, J. P.: The monsoon circulation of the Indian Ocean, *Prog. Oceanogr.*, 51, 1–123, 2001.
- Schott, F. A., Dengler, M., and Schoenefeldt, R.: The shallow overturning circulation of the Indian Ocean, *Prog. Oceanogr.*, 53, 57–103, 2002.
- Schott, F. A., Xie, S., and McCreary Jr., J. P.: Indian Ocean circulation and climate variability, *Rev. Geophys.*, 47, RG1002, doi:10.1029/2007RG000245, 2009.
- Tans, P. and Keeling, R.: Trends in atmospheric carbon dioxide, NOAA/ESRL, www.esrl.noaa.gov/gmd/ccgg/trends/ (last access: 3 December 2013), 2013.
- Takahashi, T. and Sutherland, S. C.: Final report submitted to the National Science Foundation, Washington, DC for Grant: OCE 10–38891 Climatological mean distribution of pH and carbonate ion concentration in global ocean surface waters in the unified pH scale and mean rate of their changes in selected areas, 2013.
- Takahashi, T., Sutherland, S. C., Feely, R. A., and Wanninkhof, R.: Decadal change of the surface water $p\text{CO}_2$ in the North Pacific: A synthesis of 35 years of observations, *J. Geophys. Res.*, 111, C07S05, doi:10.1029/2005JC003074, 2006.
- Takahashi, T., Sutherland, S. C., Wanninkhof, R., Sweeney, C., Feely, R. A., Chipman, D. W., Hales, B., Friederich, G., Chavez, F., Sabine, C., Watson, A., Bakker, D. C. E., Schuster, U., Metzl, N., Yoshikawa–Inoue, H., Ishii, M., Midorikawa, T., Nojiri, Y., Körtzinger, A., Steinhoff, T., Hoppema, M., Olafsson, J., Arnarson, T. S., Tilbrook, B., Johannessen, T., Olsen, A., Bellerby, R., Wong, C. S., Delille, B., Bates, N. R., and de Baar, H. J. W.: Climatological mean and decadal change in surface ocean $p\text{CO}_2$, and net sea-air CO_2 flux over the global oceans, *Deep-Sea Res. II*, 56, 554–577, 2009.
- Takahashi, T., Sutherland, S. C., and Kozyr, A.: Global ocean surface water partial pressure of CO_2 database: Measurements performed during 1957–2012 (version 2012), ORNL/CDIAC-160, NDP-088 (V2012), Carbon Dioxide Information Analysis Center, Oak Ridge National Laboratory, US Department of Energy, Oak Ridge, Tennessee, V2012, doi:10.3334/CDIAC/OTG.NDP088, available at: http://cdiac.ornl.gov/oceans/LDEO_Underway_Database/, 2013.
- Valsala, V. and Maksyutov, S.: Interannual variability of the air-sea CO_2 flux in the north Indian Ocean, *Ocean Dynam.*, 1–14, 2013.
- Valsala, V., Maksyutov, S., and Murtugudde, R.: A window for carbon uptake in the southern subtropical Indian Ocean, *Geophys. Res. Lett.*, 39, L17605, doi:10.1029/2012GL052857, 2012.
- Wakita, M., Watanabe, S., Honda, M., Nagano, A., Kimoto, K., Matsumoto, K., Kitamura, M., Sasaki, K., Kawakami, H., Fujiki, T., Sasaoka, K., Nakano, Y., and Murata, A.: Ocean acidification from 1997 to 2011 in the subarctic western North Pacific Ocean, *Biogeosciences*, 10, 7817–7827, doi:10.5194/bg-10-7817-2013, 2013.
- Wanninkhof, R.: Relationship between wind speed and gas exchange over the ocean, *J. Geophys. Res.*, 97, 7373–7382, 1992.
- Weiss, R. F.: Carbon dioxide in water and seawater: the solubility of a non-ideal gas, *Mar. Chem.*, 2, 203–215, 1974.
- Wiggert, J. D., Hood, R. R., Naqvi, S. W. A., Brink, K. H., and Smith, S. L.: Indian Ocean Biogeochemical Processes and Ecological Variability, American Geophysical Union, Washington, DC, 2009.
- Wyrski, K.: An equatorial jet in the Indian Ocean, *Science*, 181, 262–264, 1973.
- Zhang, L., Xue, L., Song, M., and Jiang, C.: Distribution of the surface partial pressure of CO_2 in the southern Yellow Sea and its controls, *Cont. Shelf Res.*, 30, 293–304, 2010.